

PHANTOM PRECIPITATION AND OTHER PROBLEMS IN TRMM PRODUCTS

Matthew Miller and Sandra Yuter

North Carolina State University, Raleigh, NC, USA

ABSTRACT

The Tropical Rainfall Measuring Mission (TRMM) satellite carries two instruments to measure precipitation: the TRMM Microwave Imager (TMI) and the Precipitation Radar (PR). Examination of instantaneous orbit data from TMI and PR reveals several problems in the TRMM products that are not readily discernible from monthly or areal averaged data sets. TMI rainfall processing algorithms yield significantly more oceanic rainfall area than the PR. Some of this areal difference is related to differences in minimum sensitivity and spatial resolution of TMI versus PR, but there are also cases where the TMI algorithms show “phantom precipitation” that is not observed by PR or ground-based radar. The TMI algorithms also produce cloud ice above the observed cloud top height for the phantom precipitation cases.

Non-physical discontinuities are frequently observed in the TMI precipitation field along the boundary between coast and ocean surface types where the weighting of the TMI channels within the algorithm changes. The discontinuities in surface rain rate are often accompanied by non-physical TMI hydrometeor profiles showing precipitation ice in rain layers below the freezing level. These non-physical profiles indicate a problem with the selection of appropriate hydrometeor profiles from the algorithm database.

Data from TMI and PR are compared on global and regional scales to identify the nature and impact of these TMI precipitation errors and the conditions under which the errors occur. It is important to identify errors and uncertainties in satellite estimates of global precipitation so that these can be taken into account in merged products and other applications of the data.

1. INTRODUCTION

Launched in 1997, the Tropical Rainfall Measuring Mission (TRMM) satellite is a joint effort of NASA and the Japanese Space Agency to improve the estimation and characterization of tropical rainfall. The TRMM satellite carries two instruments for measuring precipitation: a multi-frequency passive microwave radiometer (TRMM Microwave Imager – TMI) and a 13.8 GHz frequency precipitation radar (PR) (Kummerow et al. 1998). These instruments on the TRMM satellite allow for both simultaneous and independent measurement of storm characteristics between 35° N and 35° S latitude.

The TRMM satellite precipitation retrieval algorithms have undergone a series of refinements

since launch that have been released intermittently and labeled with different version numbers. TRMM Version 5 (V5) was released in November 1999 and Version 6 (V6), the most recent version, was released in April 2004. While the changes incorporated into each new version are intended to improve the accuracy and precision of TRMM products, they do not always do so across all metrics. The impact of precipitation retrieval errors varies with the product application. This paper will characterize several types of relative errors between the V5 and V6 PR and TMI products.

Error characteristics associated with satellite-derived precipitation products are important for the integration of TRMM products into atmospheric and hydrological model data assimilation, forecasting, and climate diagnostics applications. Additionally, this information aids in the diagnosis and refinement of physical assumptions within algorithms by identifying geographic regions and seasons where existing algorithm physics may be incorrect or incomplete. Examination of relative errors between independent estimates derived from satellite passive microwave and precipitation radar is particularly important over regions with limited surface-based measurements of rain rate such as the global oceans and tropical continents. Ground-based observations at selected sites can help guide the physical interpretation of the error characteristics. The analysis of TRMM satellite data sets yields error information on the current TRMM products and is also an opportunity to prototype error characterization methodologies for the TRMM follow-on program, the Global Precipitation Measurement mission.

A persistent problem in TRMM precipitation estimates relates to the differences in the passive microwave algorithms used over ocean, coast, and land. Examining relative errors among independent observations from TMI, PR, and surface-based observations is useful for identifying errors and inconsistencies in the measurements of the various instruments. Comparison among instruments can illustrate problems in the spatial pattern of surface precipitation intensity, the frequency distribution of precipitation rates, and the minimum detectable rain rate.

2. DATA SETS

The TRMM satellite data sets were processed to yield several types of relative error statistics in this study. We also examined the plausibility of the TRMM products compared to existing empirical knowledge. TMI and PR instantaneous rain rates are compared over ocean and land using orbit data from V6 TRMM products 2A-12, representing the TMI rainfall retrieval, and 2A-25, representing the PR rainfall retrieval.

Within the TMI instantaneous algorithm 2A-12, 85 GHz and 19 GHz are the heaviest weighted channels over ocean and land, respectively (Kummerow et al. 1996). We use the “near surface” values for rain rates, which are available in both V5 and V6 products.

Level 2 radar data from the National Climatic Data Center and the Central Weather Bureau of Taiwan was processed for comparison to TRMM products. The radar data was processed through a quality control program to unfold radial velocities and remove non-meteorological

echoes. The data was then interpolated to a 240 km by 240 km Cartesian grid with 3 km pixel resolution.

3. TMI REGIONAL PROBABILITY DENSITY FUNCTIONS (PDFs) OF RAIN RATE

The global ocean PDF is a superposition of the regional ocean PDFs. A closer look at oceanic geographic regions $\sim 2.25 \times 10^6$ km² in scale over 47-day periods showed that the degree of agreement between PR and TMI PDFs varies regionally. Some oceanic regional PDFs have become less plausible in V6 than in V5. Notably, several regional PDFs for TMI V6 ocean have a physically implausible bimodal structure (Figure 1). The corresponding PR V5 and PR V6 PDFs are unimodal. Many regions with heavy tropical precipitation during the summer season, such as the tropical western Pacific near Kwajalen, show problematic bimodal PDFs in V6 TMI (Figure 1b) that were not present in V5 (Figure 1a). Some PDFs at higher latitudes also exhibit bimodal characteristics, such as the western Atlantic off the US coast. Other PDFs have the expected unimodal characteristics, such as the southwest Pacific between the east coast of Australia and New Zealand during the local winter (Figure 1c). Figure 2 shows the geographic distribution of the various PDF modes in June and January. The bimodal PDFs occur more often in local summer months and in regions of intense

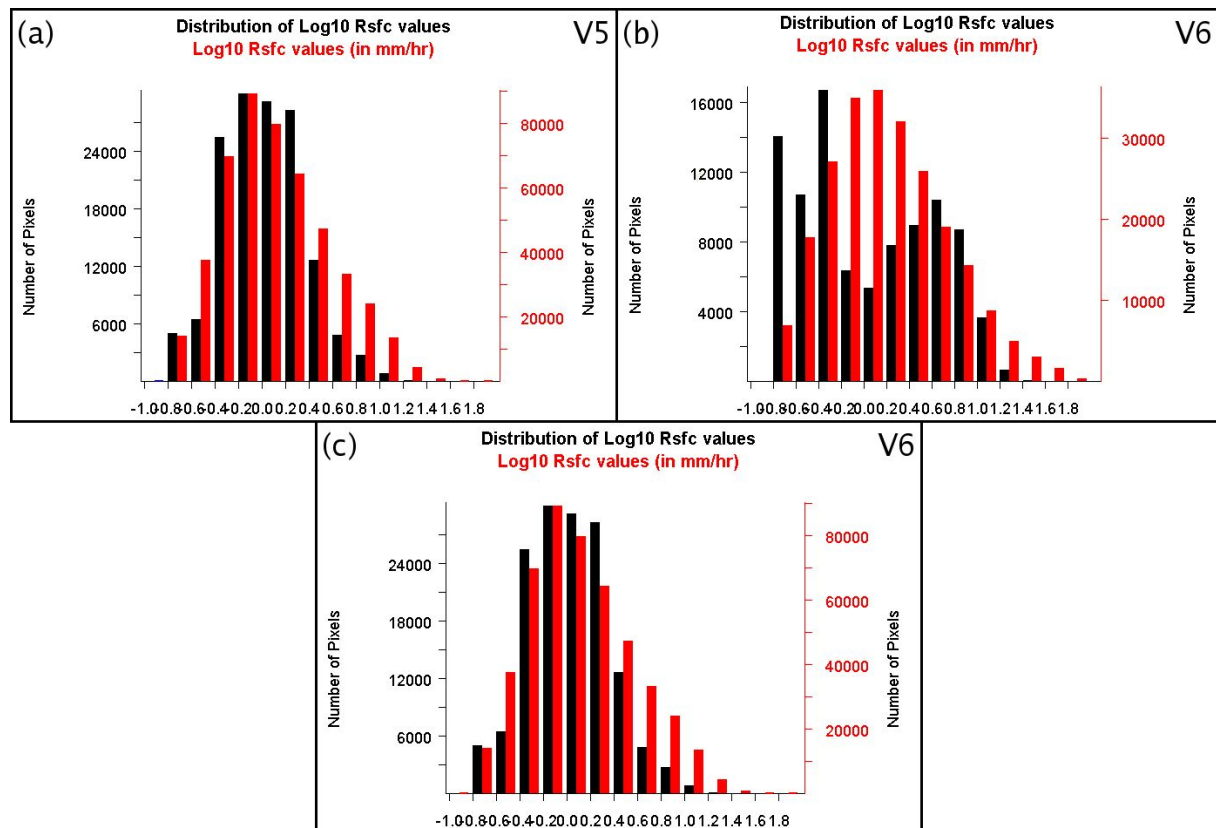


Figure 1. PDFs for TRMM V5 and V6 regional oceanic rain rates. Rain rates from PR are in grey and from the TMI swath overlapping PR are in black. PDFs represent accumulated statistics of instantaneous rain rates for 47 days of orbit products from 16 June – 1 August 2001 (pre-boost). (a) V5 Tropical Western Pacific near Kwajalein. (b) V6 Tropical Western Pacific near Kwajalein. (c) V6 Southwest Pacific between Australia and New Zealand.

precipitation such as the Intertropical Convergence Zone.

4. TMI SPATIAL DISCONTINUITIES

Over the ocean, both scattering and emission channels are used to derive the rain rate. Over the land and coast, the satellite-observed emission from precipitation is contaminated by emissions from the surface. Because the emission signal from heavy rainfall over land cannot be readily distinguished from radiation emitted from the land surface, the rainfall retrieval algorithms for the TMI must rely heavily on the scattering signal from ice. As a result, the emission channels are not weighted heavily over land and are not used at all over coast (Kummerow et al. 1996). The different sets of information available to the precipitation retrieval algorithms for land and coast versus ocean can lead to discontinuities in the retrieved precipitation field.

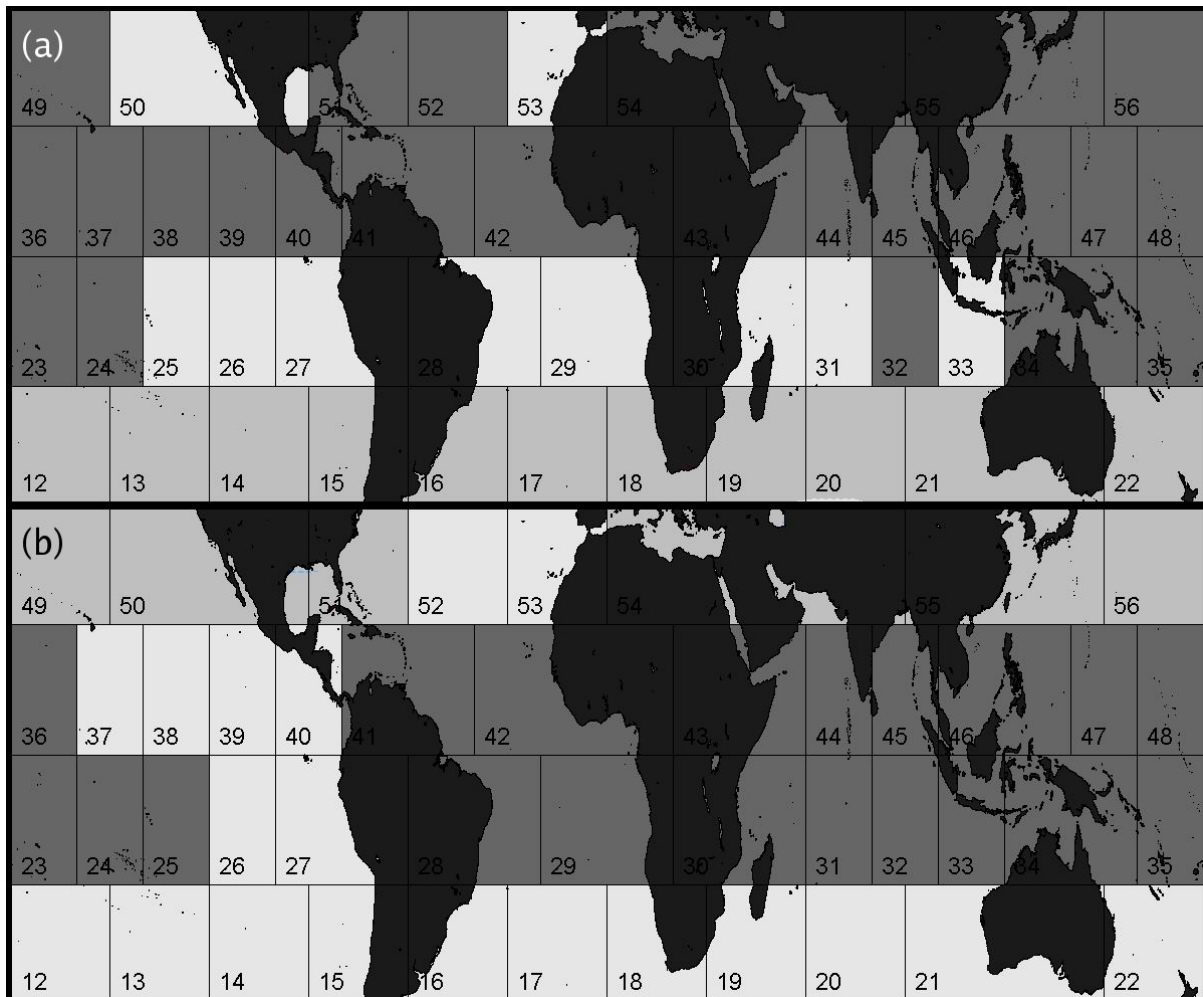


Figure. 2. Map of oceanic regional PDF shape for 47 day accumulated V6 TMI instantaneous rain rates. Color coding indicates unimodal (medium grey), bimodal (dark grey), and strongly skewed (light grey) distributions in $\log_{10}(R)$. (a) Northern Hemisphere (NH) summer from 16 June – 1 August 2001. (b) NH winter from 1 Jan – 16 Feb 2002. Grid numbers are in lower left corner of each grid box.

The TMI precipitation retrieval algorithm over the ocean differs from that over the land and coast (McCollum and Ferraro 2003). Since the TMI must rely on the signal from ice scattering over land, it can have problems detecting and determining the rain rate for shallow precipitation over land with little to no ice scattering. Figure 3 depicts a band of shallow precipitation spanning the coast of northern Morocco. The TMI is unable to detect the precipitation that lies over the coast and land surface types where the algorithm relies on an ice scattering signal. This result is not surprising when the limitations of the TMI system are considered.

However, for cases over land with a large amount of ice scattering, the TMI still has problems. Figure 4 compares the precipitation retrieval from the TRMM PR and the TMI for Hurricane Ophelia over the North Carolina coast. The TMI retrieved rain rate field has abrupt discontinuities along the boundaries between ocean and coast (Figure 4a). These discontinuities are not observed in either the TRMM PR derived rain rates or the near-surface reflectivity obtained by National Weather Service (NWS) WSR-88D radar. In the Ophelia case, the limited information from the 85.5 GHz channel leads to an underestimation of rainfall rates over land surfaces and spatial errors when locating areas of intense rainfall. The size and shape of the eye of the hurricane in the TMI rain field is also inconsistent with the PR and NEXRAD observations. Disagreement between the TMI and PR indicates observational and processing errors in one or both instruments. These inconsistencies lead to errors in the data and analyses that are derived from the TRMM observations.

Within the TMI 2A-12 algorithm, vertical profiles of hydrometeors are associated with the observed TMI brightness temperatures and estimated surface rain rates. Profiles of cloud liquid water, precipitation liquid water, cloud ice, and precipitation ice are included as part of the 2A-12 product. The hydrometeor profiles provide a valuable diagnostic of an intermediate step within the TMI algorithm.

For the Ophelia case, the freezing level is at ~4500 m altitude. Alarmingly, precipitation ice is present at altitudes below the freezing level in the TMI product over both land and ocean (Figure 4e/f). Preliminary investigation of several storms has shown that the TMI algorithm often yields erroneous precipitation ice within rain layers at altitudes well below the freezing

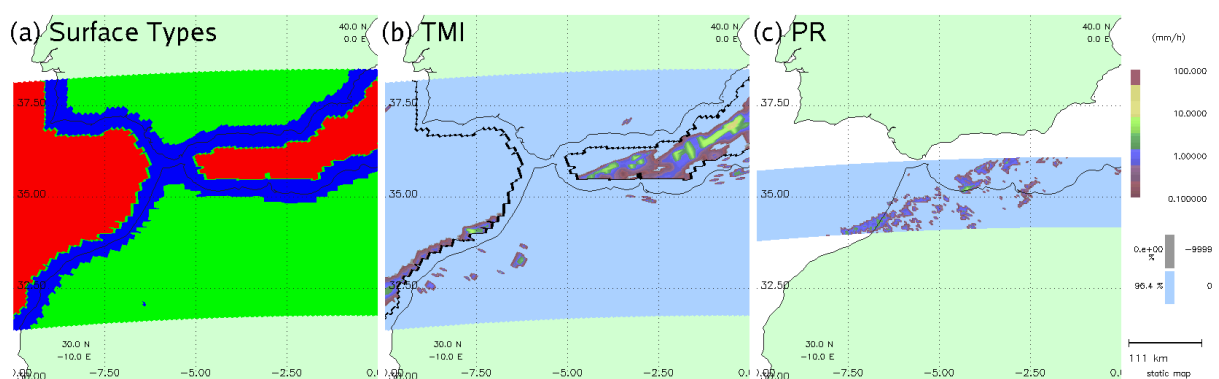


Figure 3. Shallow precipitation along the northern Morocco coast on 19 September 1999. (a) Surface masked used in 2A-12: land, coast, and ocean. (b) TMI precipitation retrieval with coast/ocean surface border overlaid. (c) PR near surface precipitation.

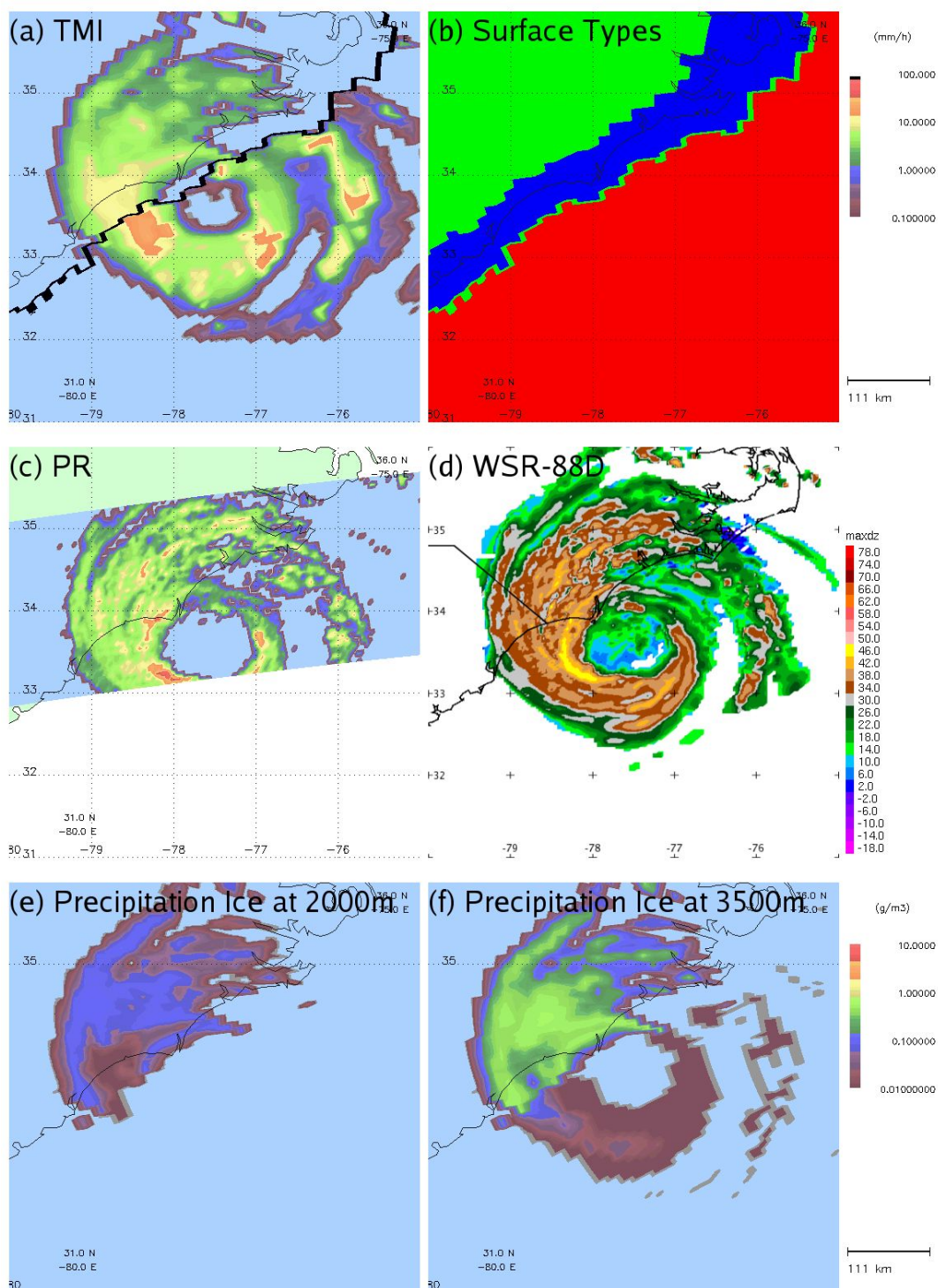


Figure 4. Views from different sensors of Hurricane Ophelia straddling the North Carolina coast at ~1400 UTC on 14 September 2005. (a) TMI precipitation retrieval with coast/ocean surface border overlaid. (b) Surface masked used in 2A-12: land, coast, and ocean. (c) PR near surface precipitation. (d) Combined radar reflectivity from coastal NWS WSR-88D radars at Morehead City, NC and Wilmington, NC. (e) TMI precipitation ice at 2000 m about the surface. (f) TRMM 2A-25 precipitation ice at 3500 m above the surface.

level. The non-physical presence of ice below the freezing level is an indication of a serious error in the TMI algorithm physics.

5. PHANTOM PRECIPITATION

Phantom precipitation is defined as a widespread area of surface precipitation over the ocean, indicated by the TMI 2A12 product, that does not exist in reality. We have identified many cases of phantom precipitation. Figure 4 shows a large area of precipitation from TMI that is not present in the corresponding PR observation. There is a unimodal distribution of rain rates in the phantom precipitation areas. Phantom precipitation rain rates can exceed 2 mm/hr and have a mode that varies from case to case ranging from 0.6 – 1.2 mm/hr. TMI returned rain rates for phantom precipitation areas lie within a range easily detectable by coastal S-band radar. Coastal S-band radar is unable to detect any precipitation return corresponding to phantom precipitation areas within observational limits (Figure 5d).

Based on analysis of IR imagery (not shown), the phantom precipitation occurs under shallow, warm topped stratus clouds. Analysis of upper-air soundings (not shown) from locations close to the phantom precipitation areas reveals cloud top heights in the 3-4km range that lie just below the freezing level. An investigation of the TMI returned hydrometeor profiles shows inconsistencies with the observed conditions. The TMI indicates a deep layer of cloud ice starting above the observed cloud top and continuing to 14-18km in height near the top of the troposphere (Figure 5c). This indicates the the TMI algorithm is returning a hydrometeor profile that is not physically consistent with the observed conditions.

A recent paper by Berg et al. (B06) investigated the differences in rainfall detection between the PR and TMI. Their study noted a large area of discrepancy over the East China Sea where the TMI was frequently signaling rain when the PR was not. B06 theorizes that aerosol loading suppresses precipitation in phantom precipitation clouds thus, lowering their reflectivity below the PR detectable threshold while maintaining a high enough liquid water path signature to be flagged as rain by the TMI algorithm. B06 offers some calculations as a proof-of-concept approach to support the plausibility of their theory. They suggest that for a relatively high liquid water content cloud with a plausible amount of aerosol loading, the reflectivity could be reduced to approximately 18 dBZ – just below the PR minimum threshold of detection.

The case examined by B06 is shown in figure 5. There is a large area of precipitation indicated by the TMI that is not present in the corresponding PR observation. An examination of the distribution of rain rates returned by the TMI (not shown) yields a unimodal distribution with a mode of approximately 1 mm/hr. This distribution of rain rates lies within the range detectable by coastal S-band radar on Taiwan. Examination of the coastal S-band radar data for the case in B06 does not reveal a widespread area of precipitation corresponding to the TMI rainfall area. The reflectivity range corresponding to the TMI rain rates as theorized by B06 would be observable by the coastal S-band radar if their echos were present.(Figure 6). The theory offered by B06 is not consistent with Taiwan coastal radar observations.

7. CONCLUSIONS

Analysis of relative errors between TMI and PR V5 and V6 data sets reveals some steps forward and backward in the TRMM algorithms. Relative differences were examined in regional and instantaneous orbit data sets. TMI and PR were compared to each other and coastal radar to identify relative errors in the TRMM observations.

Approximately half of the regional rain rate PDFs of V6 TMI oceanic rain rate exhibit an implausible bimodal distribution of rain rates that is not present in either PR V6 or V5 products. These implausible bimodal characteristics in TMI oceanic rain rate PDFs are present in a subset of the oceanic tropical and midlatitude regions, most commonly during the local summer and regions of frequent intense rainfall such as the Intertropical Convergence

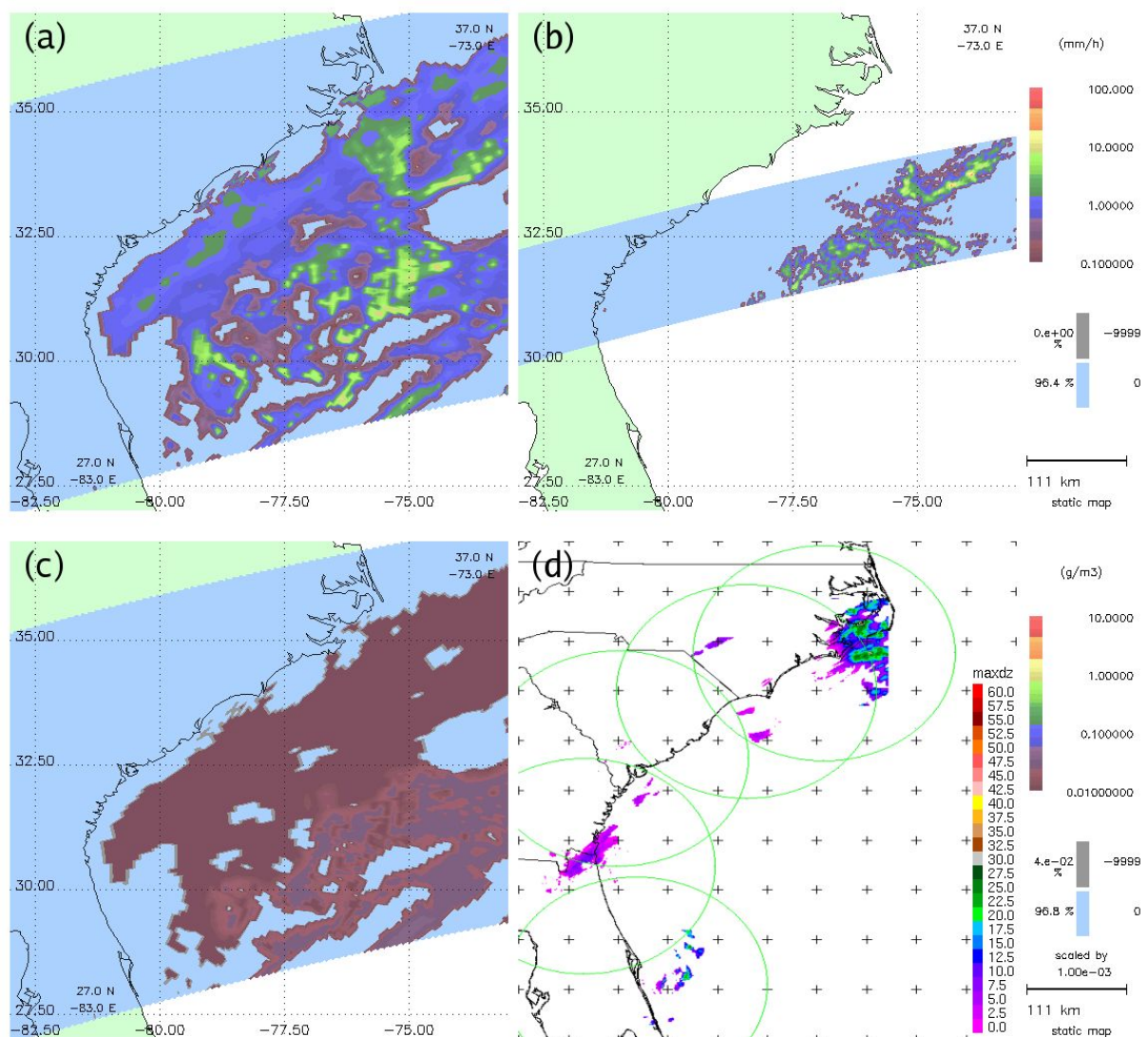


Figure 5. Phantom precipitation off the Atlantic Coast of the southeastern US on 18 March 2005. (a) TMI surface precipitation retrieval. (b) PR near surface precipitation. (c) 14km TMI cloud ice above observed cloud top level. (d) Coastal S-band radar composite. Rings denote maximum range.

Zone.

Comparison of TMI and PR data for several coastal precipitation events shows that there can be serious problems with TMI rainfall estimations at the ocean-coast boundary. The TMI had a physically implausible rain rate field that was discontinuous along the surface type boundaries between coast and ocean where the algorithm transitions from using all channels to just 85.5 GHz (Figures 3 & 4). The presence of this discontinuity along the surface type boundary signals a problem with the TMI precipitation retrieval algorithm in the cases examined.

Phantom precipitation over the ocean represents another source of error in TMI rainfall estimates. These areas of widespread precipitation in the TMI do not appear in either the PR

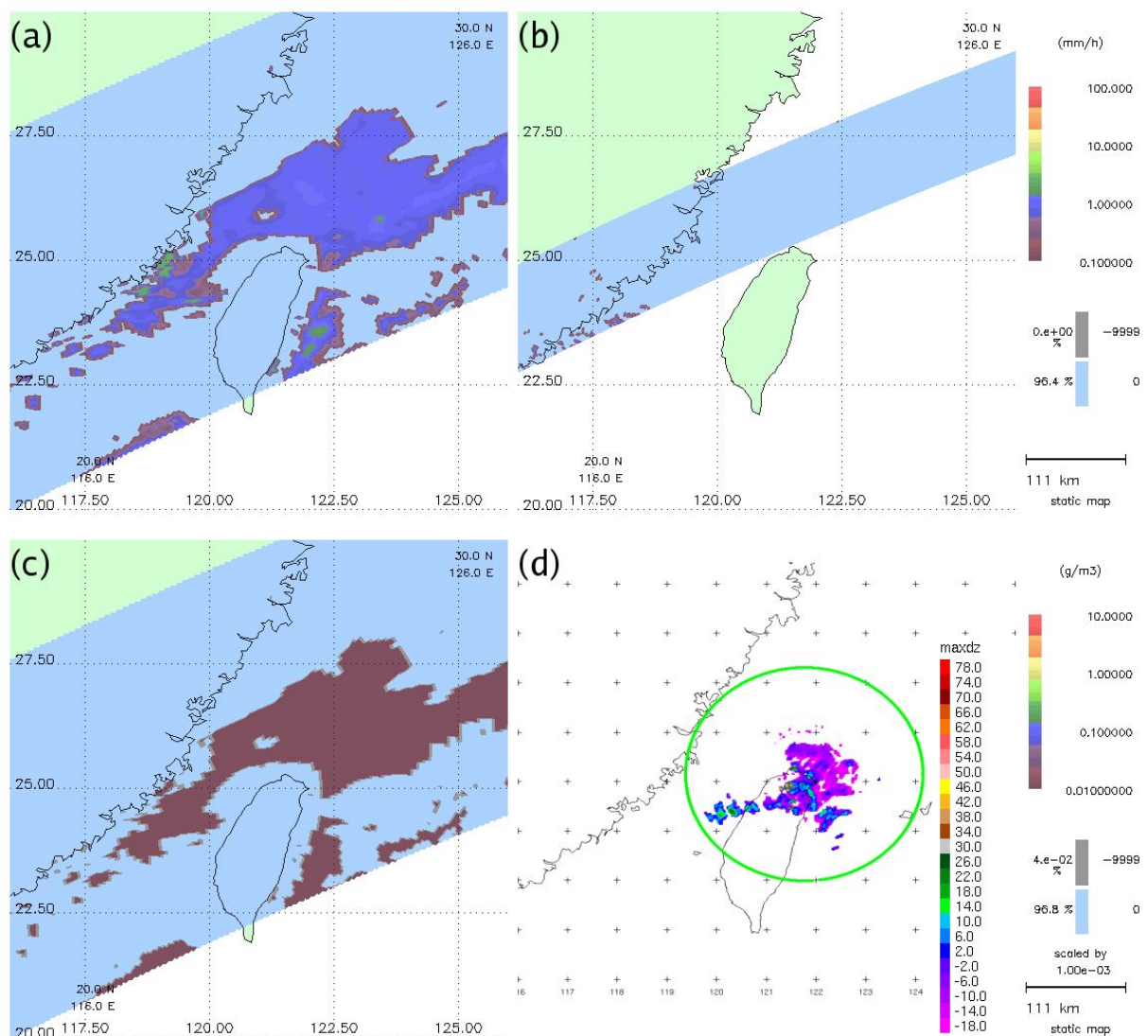


Figure 6. Phantom precipitation off the Taiwan coast on 1 Feb. 2000. (a) TMI surface precipitation retrieval. (b) PR near surface precipitation. (c) 14km TMI cloud ice above observed cloud top level. (d) Coastal S-band radar composite. Ring denotes maximum range.

or coastal S-band radar. Phantom precipitation is observed in shallow warm stratus clouds. The TMI reported rain rates for observed phantom precipitation cases can be in excess of 2 mm/hr. These cases have a unimodal rainfall distribution with modes between 0.6 and 1.2 mm/hr.

The nonphysical hydrometeor profiles observed both in situations with a coastal discontinuity in rain rates and with phantom precipitation appear to be a symptom of the TMI algorithm attempting to interpret physical conditions not well represented in its database. The TMI algorithm's hydrometeor profile – particularly the cloud ice profile - is not consistent with the observed atmosphere.

To be useful to the wider community, TRMM satellite precipitation retrievals must yield the right answers for the right reasons. Several types of relative error characteristics have improved between V5 and V6. However, changes to the TMI oceanic precipitation algorithm from V5 to V6 appear to have had unintended side effects that have degraded some regional TMI oceanic precipitation retrievals. The location and intensity of precipitation within these regions is such that these degradations are significant to global precipitation. Discontinuities in rain rates across surface type boundaries is a potential source of error in the measurement of rainfall in coastal regions. Additionally, the areas of erroneous precipitation, represented in this study as phantom precipitation, represent a problem with the TMI measurements of precipitation under certain conditions that have the potential to adversely impact water-cycle climatological studies. The problems observed in the TRMM data collected over oceanic and coastal regions need further investigation, diagnosis, and correction.

REFERENCES

- Berg, W., T. L'Ecuyer, and C. Kummerow, 2006: Rainfall Climate Regimes: The Relationship of Regional TRMM Rainfall Biases to the Environment. *J. Appl. Meteor. Climate*, **45**, 434-454
- Kummerow, C., W. S. Olson, and L. Giglio, 1996: A simplified scheme for obtaining precipitation and vertical hydrometeor profiles from passive microwave sensors. *IEEE Trans. Geosci. Remote Sens.*, **34**, 1213-1232.
- Kummerow, C., W. Barnes, T. Kozu, J. Shue, and J. Simpson, 1998: The Tropical Rainfall Measuring Mission (TRMM) sensor package. *J. Atmos. Ocean. Tech.*, **15**, 809-817.
- McCollum, J. R., and R. R. Ferraro, 2003: Next generation of NOAA/NESDIS TMI, SSM/I, and AMSR-E microwave land rainfall algorithms. *J. Geophys. Res.*, **108**, doi: 10.1029/2001JD001512.